Thermo-mechanical analysis of a DEMO divertor under the EFREMOV test conditions

Igor Simonovski*,[a], Boštjan Končar[a], Leon Cizelj[a]

[a] *Jožef Stefan Institute, Reactor Engineering Division, Jamova cesta 39, SI-1000 Ljubljana, Slovenia*

Abstract

The development of the divertor for the forthcoming DEMO fusion reactor stipulates heat flux loads larger than $10\,\mathrm{MW/m^2}$. Successful design should withstand such high loads for a number of load cycles. One of the possible divertor configurations is also a divertor concept where the cooling is provided by multiple helium cooling jets (HEMJ) (1). In this work we propose a combined computational fluid dynamics and structural model for evaluating the structural response of the HEMJ design under the EFREMOV test experimental conditions (2), designed to be close to reactor operation conditions. Heat transfer coefficients between the helium and inner surface of the thimble are first calculated using a steady state response solution. Calculated coefficients are then used as a boundary condition in a thermo-mechanical analysis of the divertor. The analysis is performed for a number of load cycles under different surface heat flux levels. Good agreement of the highest temperatures on the tile's top surface with the experimental data is obtained. The calculations suggest that there are three areas in the design where failure could initialize: a) the thimble's inner surface with the highest thermal gradients, b) tiles outer surface and c) the layer between the tile and the thimble where the temperature is higher that permissible. Post-examination data of the performed tests confirm these conclusions as cracks were observed at the above mentioned areas a) and b), while melting of the layer c) was also observed.

*Corresponding author
Email address: Igor.Simonovski@ijs.si (Igor Simonovski)

Key words: thermo-mechanical analysis, divertor, He-cooled, HEMJ concept, experiment

1. Introduction

~~A successful design of a~~ divertor ~~component for~~ the forthcoming DEMO fusion reactor ~~should~~ withstand ~~high thermal loads with~~ heat flux ~~loads~~ in excess of $10\,\mathrm{MW/m^2}$. ~~A number of~~ divertor designs have been proposed (3) ~~so far~~. Computations performed for evaluating the suitability of designs often use stipulated load conditions that are less pretentious that would be during the reactor operation. To evaluate the performance of initial designs a series of experimental tests was performed at the TSEFEY electron-beam facility of the EFREMOV Institute in Sankt Petersburg, Russia (2). These design~~ed~~ were based on ~~a divertor concept where the~~ cooling ~~is~~ provided by multiple helium cooling jets (HEMJ) (1). The applied loading conditions were designed to be as close as possible to the required design goals. The test specimen were subjected to a number of load cycles with heat flux loads ranging from $\approx 4\,\mathrm{MW/m^2}$ to above $12\,\mathrm{MW/m^2}$. Post-examination of the specimen indicated a number of cracks and small melting points at different positions (4). In this work we develop a combined computational fluid dynamics (CFD) and structural model for evaluating a HEMJ divertor under the test conditions performed at the EFREMOV Institute. The results are compared to the experimentally obtained measurements. The developed model will enable us to evaluate a number of design changes of a HEMJ divertor.

2. Divertor

A divertor exhausts the flow of energy from charged particles produced in the fusion reactions and removes helium and other impurities resulting from the reactions, and from interaction of plasma particles with the material walls (5). About 15 % of the total thermal power gained from the fusion reaction needs to be removed by divertor, resulting in an extremely high heat flux load. In

this work a HEMJ divertor, based upon a HEMJ-1c reference design, is used, Fig. 1. This design has been in development at Furschungszentrum Karlsruhe (FZK) for the last couple of years (6). Main design requirement is to remove extremely high heat flux loads of 10-15 MW/m^2. Helium is used for cooling the divertor assembly. Helium simplifies the balance of the power plant since the same coolant can be used for all internal components. Due to its chemical and neutronic inertness helium loop may be operated at higher temperatures and lower pressures than water which is used for cooling ITER divertor.

The divertor assembly itself is composed of tungsten (W) plasma-facing tile part, He-cooled thimble, made out of tungsten lanthanium oxide W-1 % La_2O_3 (WL10), and a steel cartridge that delivers multiple helium cooling jets to the thimble. Jets are used to improve the relatively low heat removal capability of helium by turbulence enhancement (7). The tile diameter is reduced from 17.8 mm (HEMJ-1c reference design) to 17.2 mm to match the size used in the experimental tests at the EFREMOV Institute (2). The thimble is brazed to the tile by a 0.05 mm layer of STEMET 1311 (Nickel based alloy), which is not modeled in this work. The thimble has an outer diameter of 15 mm and thickness of 1 mm. The outer diameter of the cartridge is 11.2 mm. The holes on the top of the cartridge have a diameter of 0.6 mm, except for the central hole which has a diameter of 1.04 mm. The gap between the thimble and the cartridge is 0.9 mm.

3. Experimental data

The cooling ability was tested experimentally at the TSEFEY electron-beam facility of the EFREMOV Institute in Sankt Petersburg, Russia (2). The facility enables testing of mock-ups at heat fluxes of up to 15 MW/m^2. During the tests the tile's top surface was heated by an electron beam of variable power level, resulting in surface heat fluxes of up to 14 MW/m^2, Fig. 2. At each power level 10 loading cycles were applied. For each cycle the beam was switched on for 30 s and then switched off for 60 s. The resulting tile's top surface temperature

at a heat flux of 11.63 MW/m^2 is given in Fig. 3 a). One can observe uneven temperature profile with approximately 26 % variation in the temperature, Fig. 3 b). The cooling helium at mass flow rates between 13.01 g/s and 13.98 g/s enters the cartridge at a constant pressure of 10 MPa. Measured helium input temperature is given in Fig. 2.

4. Model description

Two models were developed to evaluate the performance of the divertor's HEMJ-1c reference design with the tile diameter reduced to 17.2 mm. The first model is a computational fluid dynamics one where CFX software package was used (8). Amongst others, heat transfer coefficients between the helium coolant and the thimble's inner surface were calculated. Due to the computational cost of the CFD calculation the heat transfer coefficients were calculated using a steady state response solution with 11.63 MW/m^2 surface heat flux applied to the tile's top surface, helium input temperature of 558.84 ^{o}C and helium mass flow rate of 13.7 g/s. Heat transfer equations were solved simultaneously in fluid and solid domain. The shear stress transport (SST) turbulence model (9) was used to resolve turbulence and heat transfer scales in the helium flow. The SST formulation combines k-ω model to resolve near-wall turbulence and k-ϵ model for the bulk flow. Further details are given in (10). An assumption was then made that the calculated heat transfer coefficients would remain the same for different surface heat fluxes.

The second model was used to calculate the structural response. ABAQUS finite element package was used (11). Matlab interpolation function was developed to obtain the heat transfer coefficients at the nodes of ABAQUS mesh. These values were then used to define the ABAQUS wall transfer coefficient as a field variable. The applied approach enables very accurate transfer of the heat transfer coefficient from CFX to ABAQUS model, see Fig. 4. Time-dependent helium input temperature, Fig. 2, was defined as a sink temperature for the heat transfer on the thimble's inner surface. A combined thermo-mechanical analysis

was performed on the ABAQUS finite element (FE) model of the tile-thimble assembly to evaluate the resulting stresses on the assembly. Due to the symmetry only one twelfth of the model is considered. Hexagonal finite elements with 20 nodes and quadratic interpolation function were used. The influence of element size on the results was conducted as a separate study. Only minimal differences between the results were observed.

4.1. Boundary conditions

The applied loads were designed to match as closely as possible the ones of the EFREMOV experimental tests (2). The experimental surface heat flux, Fig. 2, was re-calculated from the measured helium temperature difference (the removed heat is absorbed in helium) to exclude the errors due to beam reflection and due to heat losses through the flange, where the mock-up is fixed (the real boundary condition is not adiabatic). It was then applied to the tile's top surface of the FE model, Fig. 4. Heat transfer coefficients on the thimble's inner surface, calculated using CFD model, were applied to the inner surface of the thimble, Fig. 4. Constraints were applied to the bottom surface of the thimble to prevent movement in the Z direction. Symmetry boundary conditions were prescribed on the tile and thimble front and back surfaces.

4.2. Material properties

Temperature dependent density, conductivity, thermal capacity, coefficient of thermal expansion, modulus of elasticity and Poisson ratio material data for tungsten (W) and tungsten lanthanium oxide W-1 % La_2O_3 (WL10) were taken from ITER material handbook (12). Isotropic elastic material response constitutive law was used for the tile material (W). Elastic-ideal plastic material response constitutive law was used for the thimble material (WL10). The WL10 yield stress in the temperature range from $480\,^o$C to $2000\,^o$C is tabulated in ITER material handbook. Based on these values an approximation function

$$\sigma_{yield} = 2.979 \cdot 10^{-7} \cdot T^3 - 1.176 \cdot 10^{-3} \cdot T^2 + 1.112 \cdot T + 1.305 \cdot 10^2 \qquad (1)$$

for the above temperature range is given in (12). However, below 617.8 ^{o}C the value of the approximation function begins to decrease. For temperatures lower than 617.8 ^{o}C a linear increase in yield stress was therefore assumed up to 0 ^{o}C where the yield stress was taken as 10 % higher compared to the yield stress at 617.8 ^{o}C. Above 2000 ^{o}C a constant value of yield stress was assumed. Results will show that the computed highest temperatures of the thimble are significantly lower than 2000 ^{o}C. The modified WL10 yield stress function is given with eq. (2), Fig. 5.

$$\sigma_{yield\ \mathrm{WL10}} = \begin{pmatrix} 0 \leq \mathrm{T} \leq 617.9\,^o, & -0.071 \cdot T + 482.7\,\mathrm{MPa} \\ 617.9 < \mathrm{T} \leq 2000\,^o, & \mathrm{Eq.\ (1)\,MPa} \\ 2000 < \mathrm{T}\,^o, & 33.7\,\mathrm{MPa} \end{pmatrix} \tag{2}$$

The elastic part of the elastic-ideal plastic material response curve is defined with the Young modulus. Since the data of WL10 Young modulus (E) are not available in ITER material handbook, the Young modulus of pure W was used in this part, Eq. (3). The corresponding elastic-ideal plastic material response curves for selected temperatures are given in Fig. 6.

$$E_{\mathrm{W}} = 397903 - 2.3066 \cdot T - 2.7162 \cdot 10^{-2} \cdot T \ \ \mathrm{MPa} \tag{3}$$

5. Results

Solving the thermo-mechanical problem was a two step procedure. In the first step only the thermal loads and boundary conditions were applied. In the second step the calculated temperature distribution was taken into account in the structural analysis. The calculated temperature distributions for the selected time points A, B, C, D and E are given in Fig. 7. Time points are defined in Fig. 2. Comparison between the CFX, ABAQUS and experimentally obtained highest temperatures at the tile's top surface shows a good agreement, see Table 1. Although the CFX calculations were performed as steady state approach the results are very close to ones from the ABAQUS calculation where

a unsteady approach was used. This is due to the very low frequency of the surface heat flux loads and small mass of the components involved, resulting in a quickly obtaining the thermal steady state response.

We can see that already at time point B (surface heat flux load of $6.28\,\mathrm{MW/m^2}$) the tile's top surface temperature exceeds $1100\,^o\mathrm{C}$, exceeding the tungsten re-crystallization temperature (1100-1400 ^{o}C). Reduction in mechanical strength in the affected area would therefore occur. This effect hasn't been taken into consideration in the simulation. The highest temperatures are obtained at time point E due to the highest surface heat flux ($11.62\,\mathrm{MW/m^2}$). The tile's top surface reaches $1792.1\,^o\mathrm{C}$. First possible failure of the design can also be seen. The tile and the thimble are brazed together with STEMET 1311 material at a brazing temperature of $1050\,^o\mathrm{C}$. The temperature of the brazing layer should therefore remain remain below $1050\,^o\mathrm{C}$, otherwise the delamination would occur due to the melting of the brazing layer. We can see that at the time point E the temperature is $1067.7\,^o\mathrm{C}$, see Fig. 8. Although the brazing layer itself was not modeled, including it in the analysis would not change the conclusions made sofar due to its very small thickness.

Fig. 9 shows the computed stress values. The computed stress values considerably differ compared to the ones reported in the literature so far (1; 3). The main reasons are a) higher heat flux, b) lower temperature of the cooling helium, c) higher helium mass flow rate in the presented work and d) applied ideal elastic-plastic material response constitutive law as opposed to ideal elastic. These are due to matching the loads and boundary conditions to experimental conditions. Thermal gradients and consequently computed stresses are therefore higher. The highest value of computable stress is limited by the applied elastic-ideal plastic response. The highest thermal-stress values are obtained on the thimble inner surface at a position where the helium cooling jet flow results in the highest thermal gradients. The stresses are also high at the tile's left and right outer boundary. These results are well in line with the experimental findings which show that cracks initialized at the same positions (2; 4).

The maximal principal plastic strains show that the yield stress is not ex-

ceeded only during the time points A and B, Fig. 10. At the time point C, where the surface heat flux load is $9.69\,\mathrm{MW/m^2}$, first plastic deformations develop in the areas with the highest thermal gradients. At the time points C and D (heat flux loads of 11.63 and $12.62\,\mathrm{MW/m^2}$) the plastic deformations spread to the whole circumference. For the thimble to remain within the elastic stress/strain regime at such high heat fluxes one would need to improve either the material properties or the helium cooling. One possibility would be in creating a more whirling helium-cooling flows that would decrease the thermal gradients and enlarge the regions with higher heat transfer coefficient values. In the current design these regions are very concentrated around the jet holes.

The numerical simulations indicate three problematic areas of the divertor where failure would initialize:

- The thimble inner surface where the highest equivalent stresses are observed.
- The tile's outer left and right edges where high equivalent stresses are observed.
- The brazing layer where the temperature is higher than the melting temperature of STEMET 1311.

These numerical predictions are in line with the divertor post-examination data (2; 4) where cracks at the thimble's inner surface were observed and tile's outer surface at the above mentioned position were observed. Failure of the brazing layer due to the melting was also observed, confirming the temperature in the region is too high.

6. Conclusion

A combined computational fluid dynamics and structural model is proposed for estimating the stresses and strains in divertor of the forthcoming DEMO reactor cooled with multiple helium cooling jets. Heat transfer coefficients between the helium and inner surface of the thimble are first calculated using a

steady state response solution. Calculated coefficients are then used as a boundary condition in a combined thermo-mechanical analysis of the divertor under the EFREMOV experimental test conditions. The analysis was performed for a number of load cycles under different surface heat flux levels. The calculations point to three problematic areas where failure of the design would initialize: a) the thimble inner surface in the regions with high thermal gradients b) the tile's outer left and right edges where high equivalent stresses are observed c) the brazing layer where the temperature is higher than the melting temperature of STEMET 1311. These conclusions are in line with the experimental findings (2; 4) where cracks at the thimble's inner surface and tile's outer surface at the above mentioned position were observed. Melting of the brazing layer was also observed, confirming the temperature in the region is too high.

References

[1] V. Widak, P. Norajitra, Optimization of He-cooled divertor cooling fingers using a CAD-FEM method (in press), Fusion Engineering and Design.

[2] A. Gervash, R. Giniyatulin, A. Kokoulin, A. Komarov, V. Kuznetsov, A. Makhankov, I. .Mazul, I. .Ovchinnikov, V. Smirnov, N. Yablokov, Manufacturing and testing the He-cooled target module mock-ups for DEMO fusion reactor divertor, Tech. rep., EFREMOV Institute STC Sintez St.Petersburg (2006).

[3] A. Raffray, S. Malang, X. Wang, Optimizing the overall configuration of a He-cooled W-alloy divertor for a power plant (in press), Fusion Engineering and Design.

[4] G. Ritz, T. Hirai, P. Norajitra, R. Giniyatulin, L. Singheiser, Post-examination of helium-cooled tungsten components exposed to demo specific cyclic thermal loads (in press), Fusion Engineering and Design.

[5] http://www.iter.org/, web site.

[6] P. Norajitra, A. Gervash, R. Giniyatulin, T. Ihli, W. Krauss, R. Kruessmann, V. Kuznetsov, A. Makhankov, I. Mazul, I. Ovchinnikov, He-cooled divertor for DEMO: Experimental verification of the conceptual modular design, Fusion Engineering and Design 81 (1-7) (2006) 341–346.

[7] R. Kruessmann, P. Norajitra, L. Boccaccini, T. Chehtov, R. Giniyatulin, S. Gordeev, T. Ihli, G. Janeschitz, A. Komarov, W. Krauss, R. Kruessmann, R. Kusnetzov, R. Lindau, I. Ovchinnikov, V. Piotter, M. Reith, R. Ruprecht, V. Slobodtchouk, V. Smirnov, R. Sunyk, Conceptual Design of a He-cooled Divertor with Integrated Flow and Heat Transfer promoters (PPCS subtask TW3-TRP-001-D2), Part II: Detailed Version. FZKA 6975 (accessible through http://bibliothek.fzk.de/zb/berichte/fzka6975.pdf), Tech. rep., Forschungszentrum Karlsruhe (April 2004).

[8] Ansys, CFX 11 (2007).

[9] F. Menter, Multiscale model for turbulent flows, in: 24th Fluid Dynamics Conference, American institute of aeronautics and astronautics, 1986.

[10] B. Končar, M. Draksler, P. Norajitra, V. Widak, Numerical Investigation of Multiple-Jet Cooling Concept for Helium Cooled Divertor, in: Proceedings of the International Conference Nuclear Energy for New Europe 2008, Portorož, Slovenia, September 8-11, 2008, 2008.

[11] Simulia, ABAQUS/Standard, Version 6.8-1 (2008).

[12] ITER Material Properties Handbook (2001).

LIST OF FIGURES

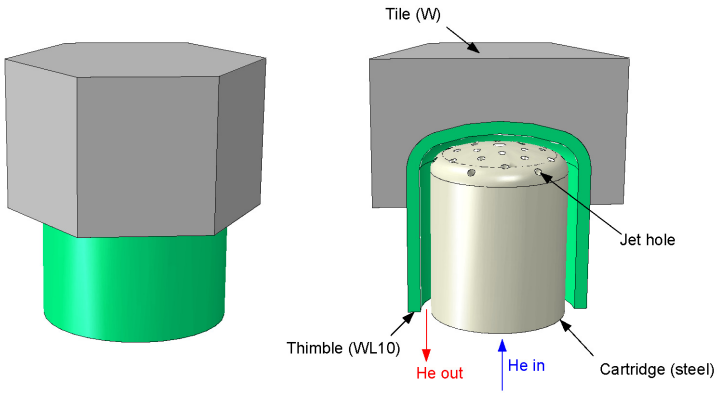

Figure 1: Schematics of the HEMJ-1c divertor finger assembly.

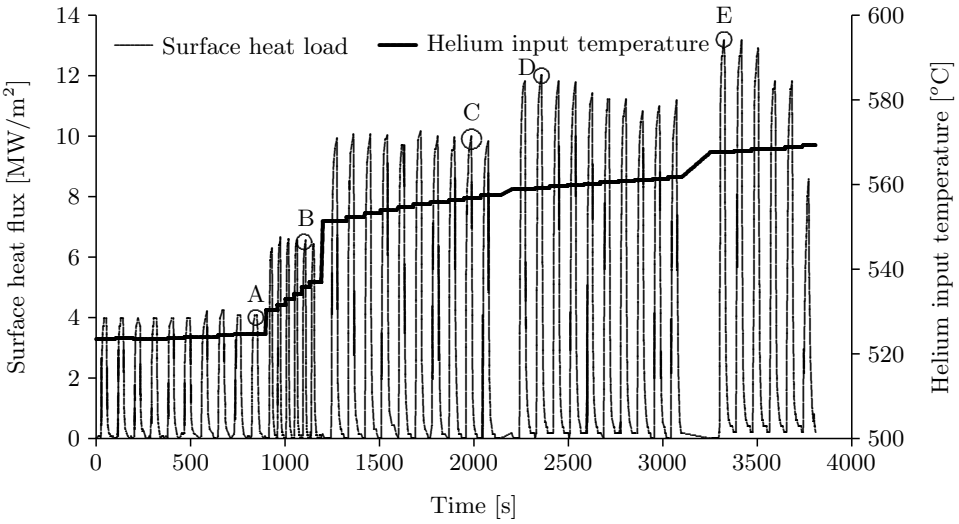

Figure 2: Surface heat flux and helium input temperature during the experiment. Results at indicated time points A-E are presented in the 'Results' section.

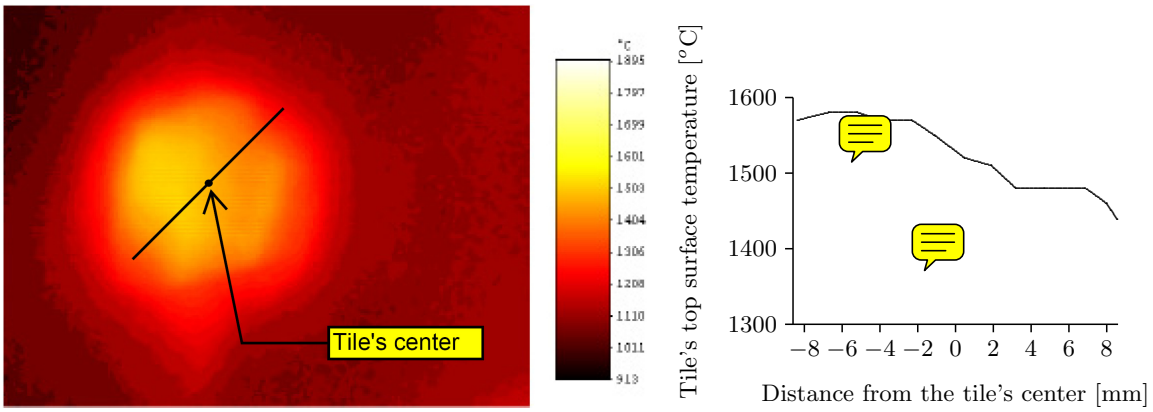

Figure 3: Tile's top surface temperature at heat flux of 11.63 MW/m^2 (2).

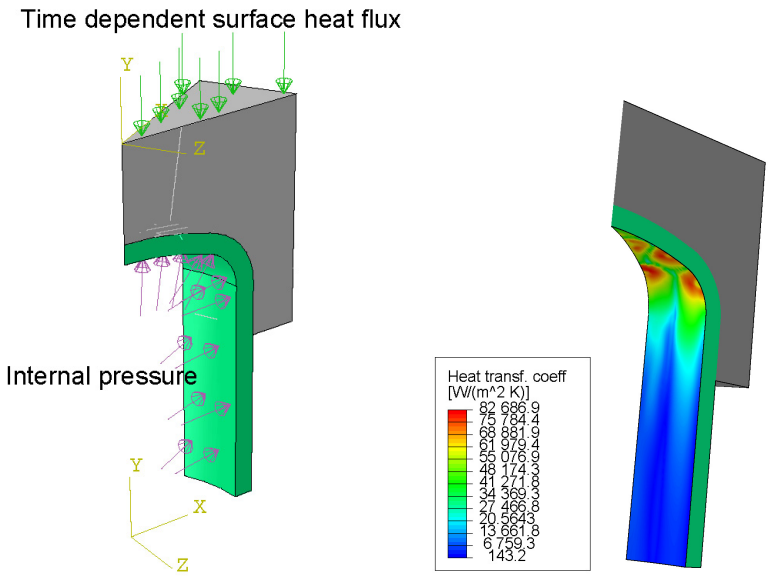

Figure 4: Applied loads and boundary conditions. Left: internal pressure and surface heat flux. Right: heat transfer coefficient at the thimble's inner surface calculated in CFX and transferred to the ABAQUS model. Green color of the thimble inside is indicative of the thimble component only.

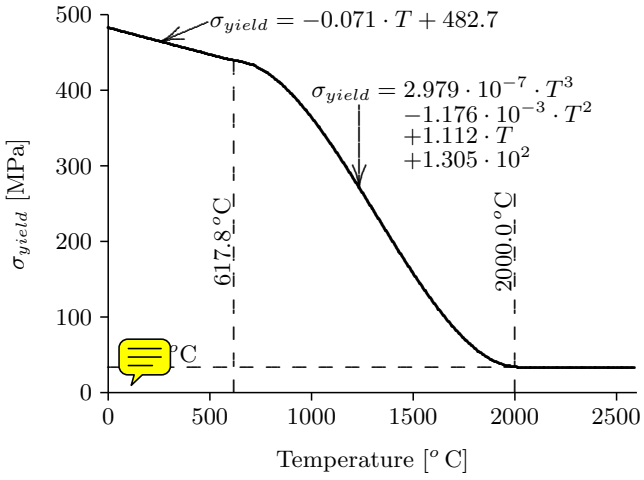

Figure 5: WL10 yield stress.

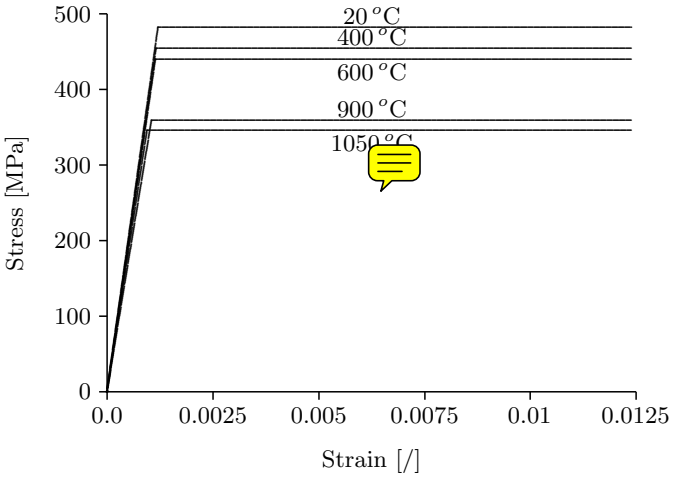

Figure 6: Elastic-ideal plastic material properties of WL10.

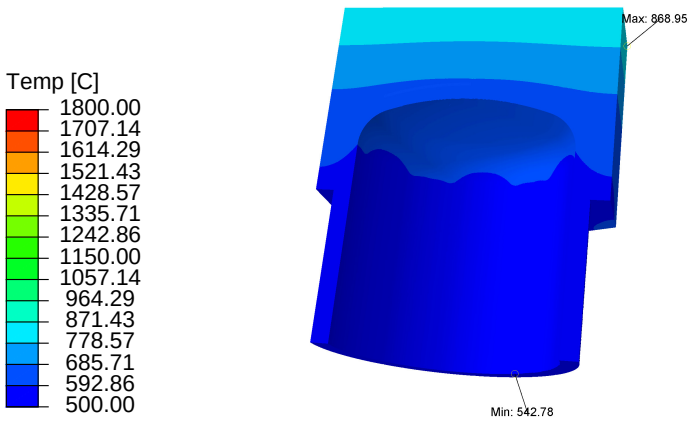

Time point A

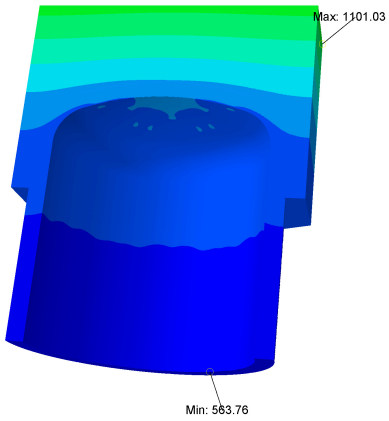

Time point B

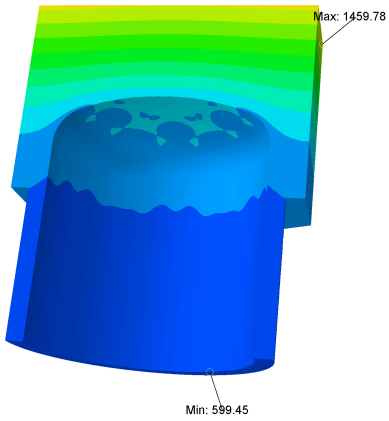

Time point C

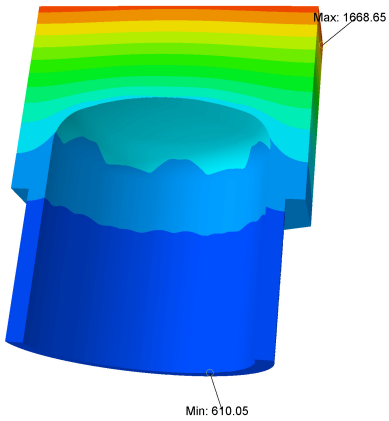

Time point D

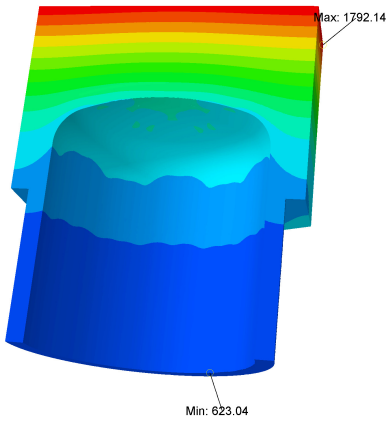

Time point E

Figure 7: Temperature distribution for time points A, B, C, D and E.

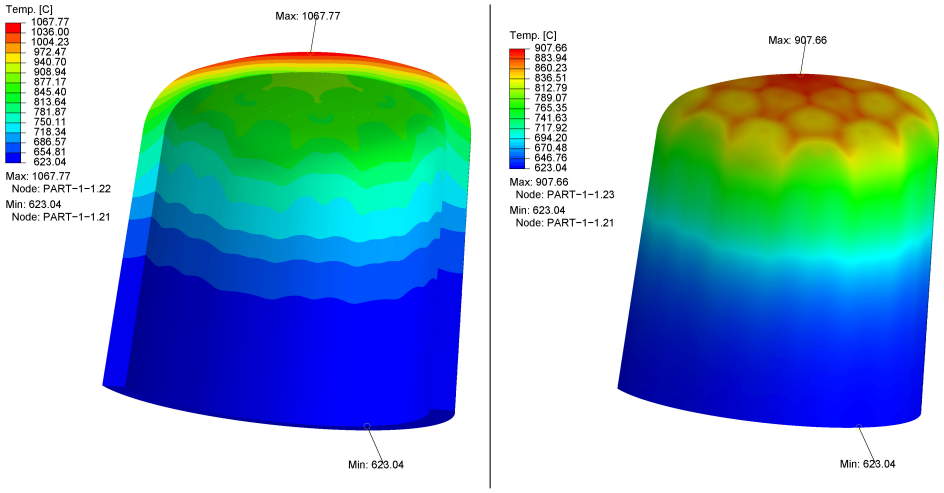

Figure 8: Thimble's temperature distribution for the time point E, right detail of the thimble's inner surface only.

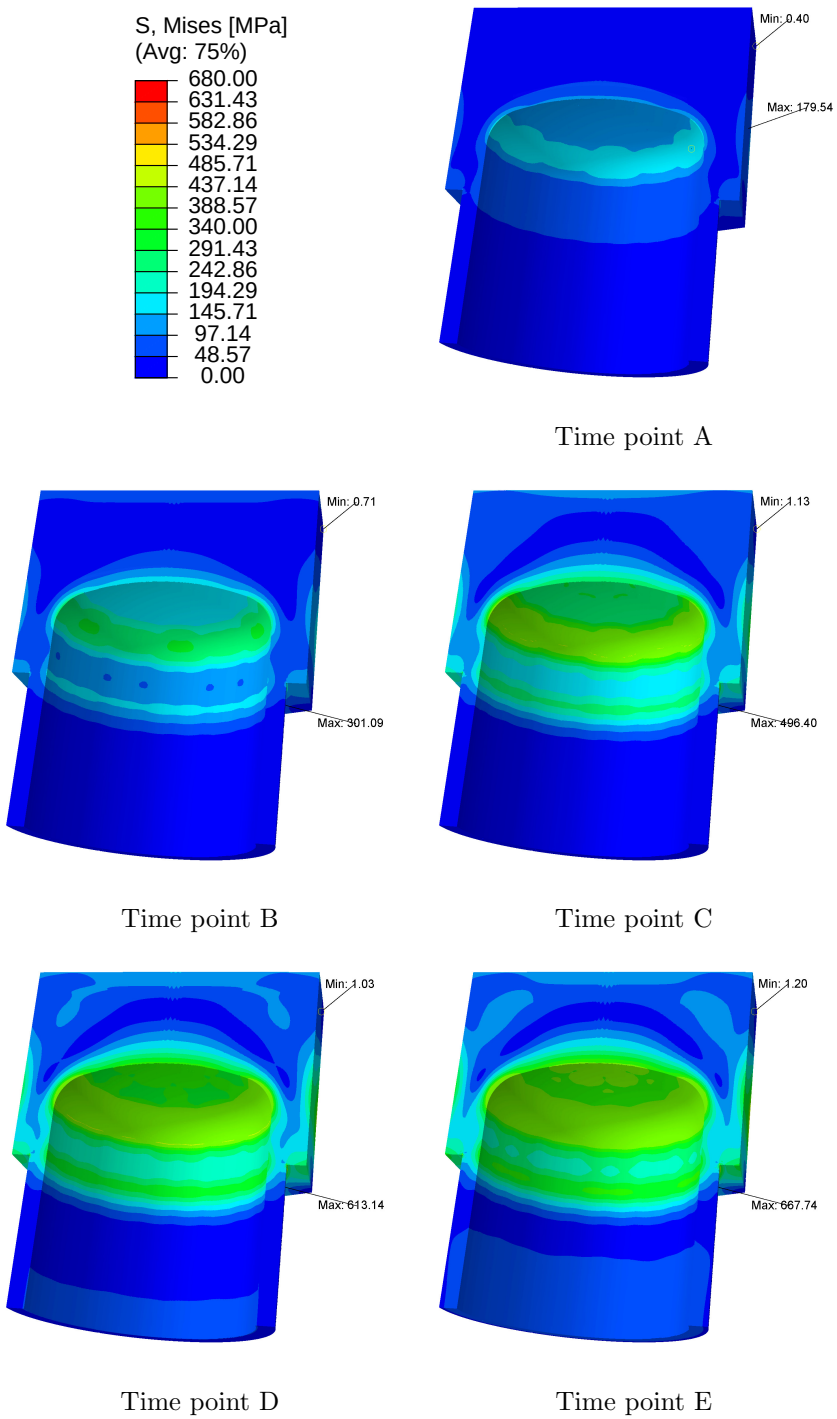

Figure 9: Mises stress distribution for time points A, B, C, D and E.

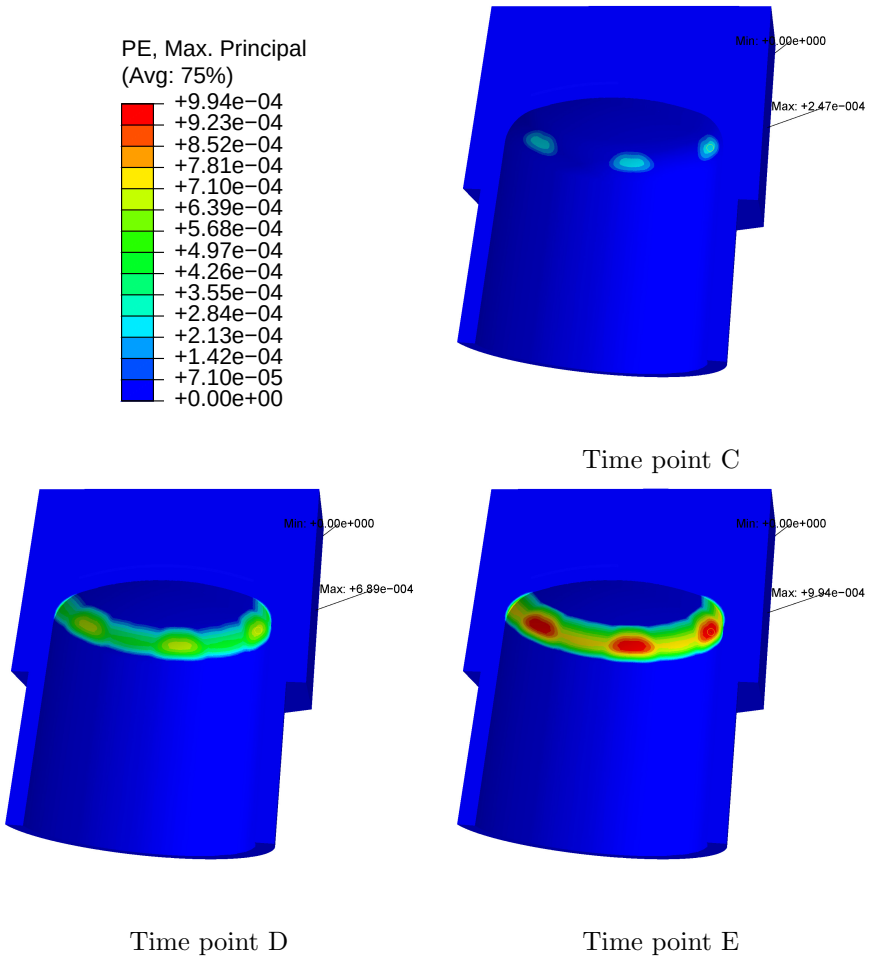

Figure 10: Maximal principal plastic strains for time points C, D and E.

LIST OF TABLES

Table 1: Comparison of values

Heat flux	Point	$\sigma_{Mises_{max}}$	$T_{Tile_{max}CFX}$	$T_{Tile_{max}ABAQUS}$	$T_{Tile_{max}Exp.}$
[MW/m^2]	[/]	[MPa]	[^{o} C]	[^{o} C]	[^{o} C]
4.01	A	179.5	866.3	868.9	941.0
6.28	B	301.1	1090.3	1101.0	1153.0
9.69	C	496.7	1447.3	1459.8	1424.0
11.63	D	617.6	1648.6	1668.6	1597.0
12.62	E	678.58	1765.9	1792.1	1788.0